IJMMM International Journal of Minerals, Metallurgy and Materials 矿物冶金与材料学报（英文版）

Synthesis, characterization and magnetic properties of $KFeO_2$ nanoparticles prepared by a simple egg white solution route

Thongsuk Sichumsaeng, Nutthakritta Phromviyo, Supree Pinitsoontorn, Pinit Kidkhunthod, Narong Chanlek, and Santi Maensiri

Cite this article as:
Thongsuk Sichumsaeng, Nutthakritta Phromviyo, Supree Pinitsoontorn, Pinit Kidkhunthod, Narong Chanlek, and Santi Maensiri, Synthesis, characterization and magnetic properties of $KFeO_2$ nanoparticles prepared by a simple egg white solution route, *Int. J. Miner. Metall. Mater.*, 29(2022), No. 1, pp. 128-135. https://doi.org/10.1007/s12613-020-2194-x

---

Articles you may be interested in

Fan Zeng, Xue-jiao Bai, Cheng-liang Hu, Min-jun Tang, and Zhen Zhao, Effect of plastic strain and forming temperature on magnetic properties of low-carbon steel, *Int. J. Miner. Metall. Mater.*, 27(2020), No. 2, pp. 210-219. https://doi.org/10.1007/s12613-019-1905-7

Bo Liu, Shen-gen Zhang, Britt-Marie Steenari, and Christian Ekberg, Synthesis and properties of $SrFe_{12}O_{19}$ obtained by solid waste recycling of oily cold rolling mill sludge, *Int. J. Miner. Metall. Mater.*, 26(2019), No. 5, pp. 642-648. https://doi.org/10.1007/s12613-019-1772-2

Shuang Huang, Hua-lan Xu, Sheng-liang Zhong, and Lei Wang, Microwave hydrothermal synthesis and characterization of rare-earth stannate nanoparticles, *Int. J. Miner. Metall. Mater.*, 24(2017), No. 7, pp. 794-803. https://doi.org/10.1007/s12613-017-1463-9

Li-ping Wang, Fu Zhang, Shuai Chen, and Zi-heng Bai, One-pot synthesis and optical properties of In-and Sn-doped ZnO nanoparticles, *Int. J. Miner. Metall. Mater.*, 24(2017), No. 4, pp. 455-461. https://doi.org/10.1007/s12613-017-1426-1

Shi-na Li, Rui-xin Ma, and Cheng-yan Wang, Solid-phase synthesis of Cu_2MoS_4 nanoparticles for degradation of methyl blue under a halogen-tungsten lamp, *Int. J. Miner. Metall. Mater.*, 25(2018), No. 3, pp. 310-314. https://doi.org/10.1007/s12613-018-1574-y

Seyed Rahim Kiahosseini and Hossein Ahmadian, Effect of residual structural strain caused by the addition of Co_3O_4 nanoparticles on the structural, hardness and magnetic properties of an Al/Co_3O_4 nanocomposite produced by powder metallurgy, *Int. J. Miner. Metall. Mater.*, 27(2020), No. 3, pp. 384-390. https://doi.org/10.1007/s12613-019-1917-3

IJMMM WeChat

QQ author group

International Journal of Minerals, Metallurgy and Materials
Volume 29, Number 1, January 2022, Page 128
https://doi.org/10.1007/s12613-020-2194-x

Synthesis, characterization and magnetic properties of $KFeO_2$ nanoparticles prepared by a simple egg white solution route

Thongsuk Sichumsaeng[1,2,3], *Nutthakritta Phromviyo*[1], *Supree Pinitsoontorn*[4], *Pinit Kidkhunthod*[5], *Narong Chanlek*[5], *and Santi Maensiri*[1,2,3]✉

1) School of Physics, Institute of Science, Suranaree University of Technology, Nakhon Ratchasima, 30000, Thailand
2) SUT CoE on Advanced Functional Materials, Suranaree University of Technology, Nakhon Ratchasima, 30000, Thailand
3) Research Network NANOTEC-SUT on Advanced Nanomaterials and Characterization, Suranaree University of Technology, Nakhon Ratchasima, 30000, Thailand
4) Department of Physics, Faculty of Science, Khon Kaen University, Khon Kaen, 40002, Thailand
5) Synchrotron Light Research Institute (Public Organizer), Nakhon Ratchasima, 30000, Thailand
(Received: 3 July 2020; revised: 8 September 2020; accepted: 11 September 2020)

Abstract: Nanoparticles of potassium ferrite ($KFeO_2$) in this work were synthesized by a simple egg white solution method upon calcination in air at 773, 873, and 973 K for 2 h. The effects of calcination temperature on the structural and magnetic properties of the synthesized $KFeO_2$ nanoparticles were investigated. By varying the calcination temperature, X-ray diffraction and transmission electron microscopy results indicated the changes in crystallinity and morphology including particle size, respectively. Notably, the reduction in particle size of the synthesized $KFeO_2$ was found to have a remarkable influence on the magnetic properties. At room temperature, the synthesized $KFeO_2$ nanoparticles prepared at 873 K exhibited the highest saturation magnetization (M_S) of 2.07×10^4 A·m^{-1}. In addition, the coercivity (H_C) increased from 3.51 to 16.89 kA·m^{-1} as the calcination temperature increased to 973 K. The zero-field cooled (ZFC) results showed that the blocking temperatures (T_B) of about 125 and 85 K were observed in the samples calcined at 773 and 873 K, respectively. Therefore, this work showed that the egg white solution method is simple, cost effective, and environmentally friendly for the preparation of $KFeO_2$ nanoparticles.

Keywords: egg white solution method; potassium ferrite nanoparticles; magnetic properties; ferromagnetism

1. Introduction

Over the past few decades, magnetic materials have been explored in various fields of applications [1–4]. Depending on the synthetic methods, different types of magnetic materials such as Fe-based nanoparticles show interesting properties [5–8]. Alkaline metal ferrites with the general formula $AFeO_2$ (where A = Li, Na, K) have been extensively studied because they offer many applications, especially in rechargeable lithium batteries [9–11]. Potassium ferrite ($KFeO_2$) is an interesting alkaline metal ferrite, which has been widely used as a catalyst for dehydrogenation [12] and cathode material for potassium-ion batteries [13]. Recently, $KFeO_2$ nanoparticles showed potential application as photoanode in dye-sensitized solar cells due to their narrow band gap [14]. The combination of potassium with iron-based compounds has resulted in biocompatible materials because of their inherent non-toxicity [15]. For metal removal applications, $KFeO_2$ shows potential as a magnetic sorbent for Cu^{2+} removal [16]. Therefore, various methods have been applied to synthesize $KFeO_2$ nanoparticles including solid-state [13], sol–gel [17–18], combustion [19], conventional ceramic [20], and ball-milling [21]. Among these methods, the solution method is promising for the preparation of $KFeO_2$ nanoparticles due to its low temperature, short reaction time, and homogeneous mixing [22]. In a typical sol–gel method, the stable solution or sol forms after materials undergo hydrolysis, and the gel resulting from a polycondensation reaction occurs after gelation [23–24].

Egg white is one of the main components in hen egg, which mainly contains about 92% of proteins [25]. Ovalbumin is known as the major protein in egg white; it has four free sulfhydryl (SH) groups and one disulfide (SS) bond [26]. Upon heating, these SH groups rapidly initiate polymerization through SH–SS exchange reactions, thereby interconnecting different egg white proteins [27]. As a result, a continuous network is formed. In the preparation of nanocrystalline materials, egg white protein (ovalbumin) is attracting considerable attention because of its excellent characteristic such as gelling, forming, and emulsifying [28]. As a result of its water solubility and its ability to associate with metal ions in solution, egg white proteins have been used as a binder cum gel for shaping bulk and porous ceramic materials [29]. Moreover, egg white has been used as a capping agent for

✉ Corresponding author: Santi Maensiri E-mail: antimaensiri@gmail.com, santimaensiri@g.sut.ac.th

template growth and organization of nanoparticles [30]. The synthesis of $KFeO_2$ nanoparticles using the egg white solution method and the dependence of magnetic properties on the calcination temperature have not been reported yet.

In this work, we report a simple, low cost, and eco-friendly synthesis of $KFeO_2$ nanoparticles via the egg white solution method. The crystal structure, morphology, chemical compositions, and valence state of the synthesized $KFeO_2$ were characterized by X-ray diffraction (XRD), transmission electron microscopy (TEM), X-ray photoelectron spectroscopy (XPS), and X-ray absorption near edge spectroscopy (XANES), respectively. Vibrating sample magnetometer (VSM) measurements were performed on the synthesized $KFeO_2$ nanoparticles to determine their magnetic properties. The dependence of magnetic properties on calcination temperature was also investigated and discussed.

2. Experimental

2.1. Synthesis of $KFeO_2$ nanoparticles

In this work, $KFeO_2$ nanoparticles were synthesized by a simple egg white solution method. The starting materials of KNO_3 (Prolabo, 99.9%), $Fe(NO_3)_3 \cdot 9H_2O$ (Sigma-Aldrich, 99.99%), and freshly extracted chicken egg white (ovalbumin) were used without further purification. First, freshly extracted egg white (60 mL) was mixed with deionized water (40 mL) under vigorous stirring to obtain a binder cum gel. Second, KNO_3 and $Fe(NO_3)_3 \cdot 9H_2O$ in a molar ratio of 1:2 were slowly added to the egg white solution until the homogenous solution was obtained. The mixture was evaporated by heating on a hotplate at 353 K until the dried precursor was obtained. To obtain $KFeO_2$ powder, the dried precursor was crushed and calcined in a box furnace with a heating rate of 5 $K \cdot min^{-1}$ at 773, 873, and 973 K for 2 h. The schematic preparation of $KFeO_2$ nanoparticles by using the egg white solution method is presented in Fig. 1.

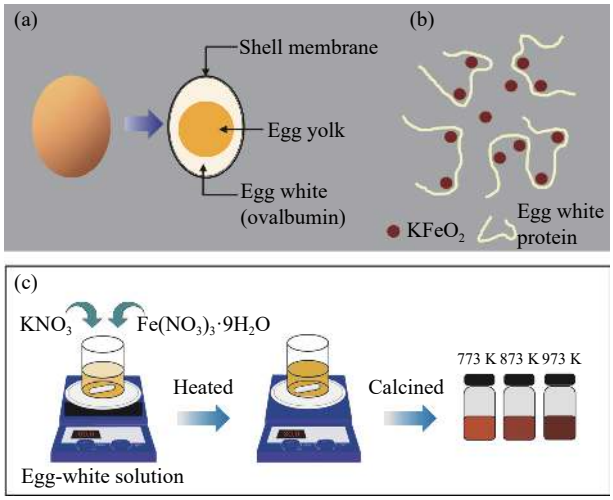

Fig. 1. (a) Components of chicken egg, (b) possible formation of egg white protein surrounding $KFeO_2$ nanoparticles, and (c) schematic preparation of $KFeO_2$ nanoparticles using the egg white solution method.

2.2. Characterization

The crystal structure and phase purity of the synthesized $KFeO_2$ nanoparticles were characterized by XRD (Bruker D8) with Cu K_α radiation (λ = 0.15406 nm) at scanning rate of 0.02°·min^{-1} in the 2θ range between 10° and 70°. Rietveld refinements were carried out with JANA2006 software [31] by using pseudo-Voigt or the combination of Lorentzian and Gaussian profile functions. The standard crystallographic information file (CIF) of orthorhombic $KFeO_2$ structure with space group of Pbca was taken from the literature [32] and used for refinement. The morphology including particle size was revealed by TEM (JEOL EM-902). To examine the chemical compositions of the synthesized $KFeO_2$ nanoparticles, XPS was carried out with the PHI Versa Probe II XPS system (ULVAC-PHI) with Al K_α radiation at the SUT-NANOTEC-SLRI joint research facility, Synchrotron Light Research Institute, Thailand. The C 1s peak at 284.5 eV was used as a reference to calibrate the binding energy (BE) for XPS measurements. The valence states of K and Fe atoms in all the synthesized samples were investigated by XANES in transmission mode at BL5.2: SUT-NANOTEC-SLRI, Synchrotron Light Research Institute, Thailand. In addition, magnetic properties of the synthesized $KFeO_2$ nanoparticles at different calcination temperatures were studied via VSM (Lake Shore 7403) measurements.

3. Results and discussion

3.1. Structural analysis

Fig. 2(a) shows the powder XRD patterns of the as-synthesized $KFeO_2$ and the synthesized $KFeO_2$ samples calcined at 773, 873, and 973 K. The XRD results of the as-synthesized sample show the phase formation of KNO_3, which originated from the starting material. The XRD patterns of all the calcined samples are well matched with an orthorhombic $KFeO_2$ structure (file No. 83-2152). Additionally, XRD patterns show that peak shape and intensity are strongly affected by the calcination temperature. The reduction of peak intensity is related to the decrease in crystallinity in the sample calcined at high temperatures [33]. The secondary phase of KNO_2 is also found in all the calcined samples, which possibly originated from the thermal decomposition of KNO_3 [34]. Moreover, the structural information of $KFeO_2$ samples calcined at different temperatures was investigated by using Rietveld refinement. As a result, the quality of the structural refinement is indicated by residual functions of profile factor (R_p), weighted profile residual (R_{wp}), expected R-value (R_{exp}), and goodness of fit (GoF) [35]. R_p is related to the residual error, which was directly calculated from the structural model of the XRD patterns and the experimental data. R_{wp} is the weight of the particular location based on R_p [36]. GoF or the "chi square" (χ^2) is defined as the minimization function, which is determined from the square of the ratio between R_{wp} and R_{exp}. Fig. 2(b) shows the refinement plot of $KFeO_2$ sample calcined at 773 K. It is clearly observed in Fig. 2(b) that the values of R_p and R_{wp} were under 15%, indic-

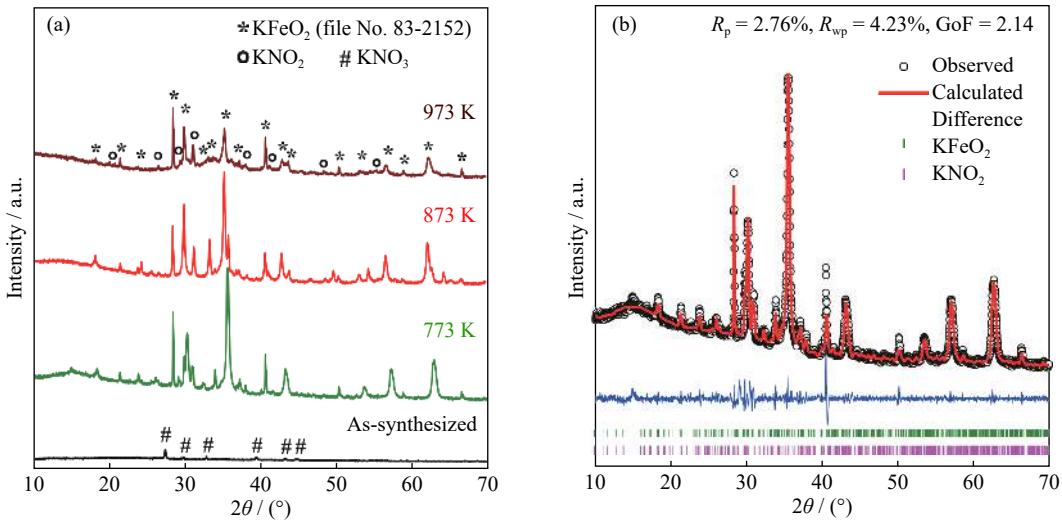

Fig. 2. (a) XRD patterns of as-synthesized $KFeO_2$ and $KFeO_2$ calcined at different temperatures and (b) sample Rietveld refinement plot of $KFeO_2$ calcined at 773 K with R_p, R_{wp}, and GoF.

ating that the Rietveld refinement results are reliable [37].

3.2. Morphological analysis

TEM bright-field images of the as-synthesized $KFeO_2$ and the synthesized $KFeO_2$ samples calcined at different temperatures are shown in Fig. 3. The TEM bright-field images reveals the difference in morphology between the as-synthesized and $KFeO_2$ samples calcined at 773, 873, and 973 K. Fig. 3(a) shows a typical TEM image of the as-synthesized $KFeO_2$ sample, which reveals the formation of an egg white network. This formation could be caused by the evaporation of water molecules at the drying gel process. The network is partially destroyed, leaving a cube-like shape of $KFeO_2$ nanoparticles after calcination as clearly seen in Fig. 3(b) and (c). Besides, the particle size of the synthesized $KFeO_2$ strongly depends on the calcination temperature. As the calcination temperature increases, the size of nanoparticles decreases and converts into an agglomerated form after calcination at 973 K (Fig. 3(d)). The increase in surface energy results in an increase in surface interactions of the samples calcined at 973 K [17]. The average particle sizes of the samples calcined at 773 and 873 K were estimated to be 57 and 38 nm, respectively. Therefore, the TEM results clearly indicate the role of egg white solution as binder cum gel for shaping materials.

3.3. XPS analysis

Fig. 4(a) shows the survey XPS spectra of the calcined $KFeO_2$ samples. Carbon (C), potassium (K), oxygen (O), and iron (Fe) are presented on the sample surface. The intensity of Fe peaks decreases with increasing calcination temperature.

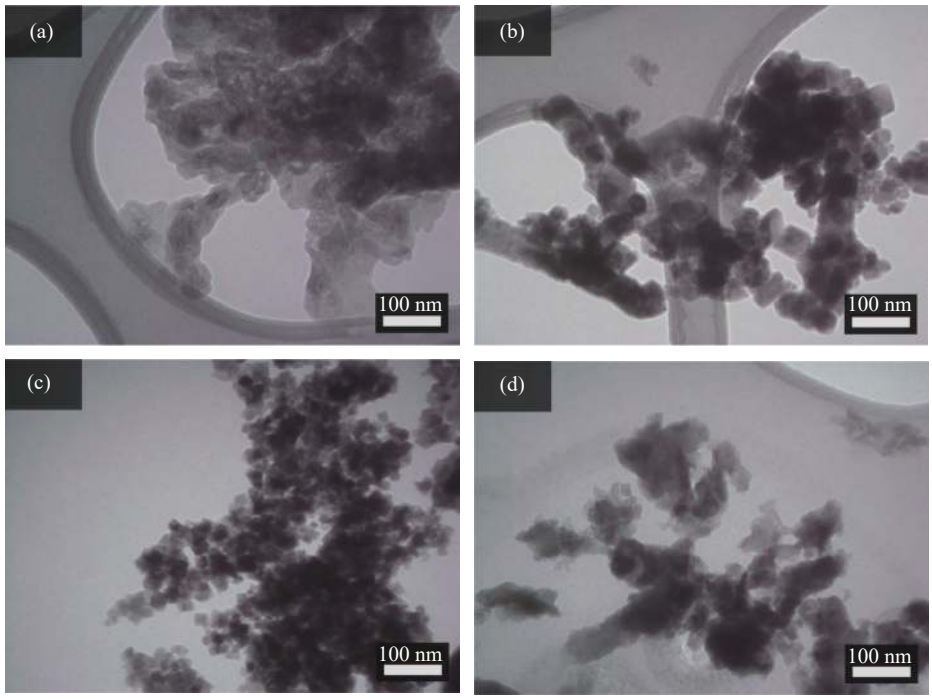

Fig. 3. TEM bright-field images of (a) the as-synthesized and (b–d) $KFeO_2$ samples calcined at (b) 773 K, (c) 873 K, and (d) 973 K for 2 h.

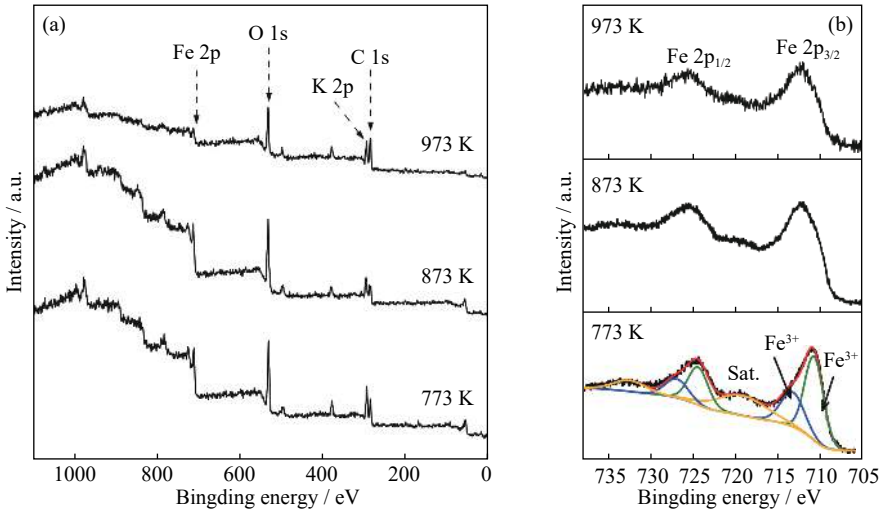

Fig. 4. Survey XPS spectra (a) and high-resolution XPS spectra in the Fe 2p region (b) of the $KFeO_2$ samples calcined at 773, 873, and 973 K for 2 h. Sat. is satellite peak.

This trend implies that the atomic concentration of Fe on the sample surfaces decreases when the calcination temperature increases. The relative atomic concentrations of the synthesized $KFeO_2$ samples calcined at different temperatures are given in Table 1. The high-resolution XPS spectra in the Fe 2p regions are also shown in Fig. 4(b). Peaks at all the spectra are intense peaks at the BE of 711.2 and 724.5 eV, as well as satellite at 720.0 eV. These findings are consistent with the presence of Fe^{3+} in the calcined samples [38].

Table 1. Relative atomic concentration of the synthesized $KFeO_2$ samples calcined at different temperatures %

Calcined temperature / K	C	O	K	Fe
773	24.84	43.43	8.74	22.99
873	23.01	45.70	7.16	24.12
973	45.19	37.01	7.92	9.87

3.4. XANES analysis

The valence states of K and Fe in all the calcined samples were determined by the XANES spectra, which were measured at the K K-edge and Fe K-edge, respectively. The peak position, intensity, and shape of the XANES spectra depend on the local electronic structure of the absorbing atom, which provides information on the absorbing valence state [39]. Fig. 5(a) shows the normalized XANES spectra of the potassium iodide (KI) standard (std.) sample and $KFeO_2$ samples calcined at 773, 873, and 973 K. As shown in Fig. 5(a), the edge energies at the K K-edge of all the calcined samples are similar to the edge energy of the KI standard sample, indicating that the valence state of K atom in these samples is 1+. These results are also confirmed by their first derivative plots shown in Fig. 5(b). At the Fe K-edge, the normalized XANES spectra of all the calcined samples and the reference compounds of FeO, Fe_2O_3, and Fe_3O_4 are presented in Fig. 5(c). As shown in Fig. 5(c), the XANES spectra can be divided into the two following regions [40–41]: (i) the pre-edge region at low energy is attributed to the 1s → 3d transition; (ii) the sharp rise of the absorption at the second region is related to the 1s → 4s transition. In region I, the pre-edge peak of Fe at a certain energy has been widely used to determine its valence state [42]. In comparison with the reference compounds, the energy positions of all the calcined samples are quite similar with the energy position of the Fe_2O_3 standard compound, implying that the valence state of Fe in theses samples is 3+. In region II, the absorption edge energies of all the calcined samples are found to match very well with the edge energy of the Fe_2O_3 standard compound, confirming that the valence state of Fe is 3+. This result is consistent with their first derivative plots presented in Fig. 5(d). Therefore, the XANES results prove the absence of significant changes in local electronic structure with increasing calcination temperatures.

3.5. Magnetic properties

Fig. 6(a) shows the magnetization as a function of the applied magnetic field (±1600 $kA \cdot m^{-1}$) of all the calcined $KFeO_2$ samples obtained from the VSM measurement at room temperature. As illustrated in Fig. 6(a), the magnetization of all the calcined samples increases with increasing applied magnetic field. As the magnetic field further increases, the saturation magnetization (M_S) is reached. The highest M_S value is found to be 2.07×10^4 $A \cdot m^{-1}$ in the sample calcined at 873 K, and this value is slightly higher than the value of 2.03×10^4 $A \cdot m^{-1}$ in the sample prepared by the sol–gel method [15]. In addition, the M_S value of the calcined $KFeO_2$ sample increases with increasing calcination temperature and decreased thereafter. High M_S values are due to the high magnetic moment involved in small particle size as observed by TEM [43]. Interestingly, the M_S values found here correlate well with the relative atomic concentrations of carbon (C) and iron (Fe) as summarized in Table 1. Regarding the magnetic nanoparticles, the two main factors that dominate magnetic properties of nanoparticles are finite size effects and surface effect [44]. Thus, the low M_S value of the synthesized $KFeO_2$ may be explained by the surface effect because

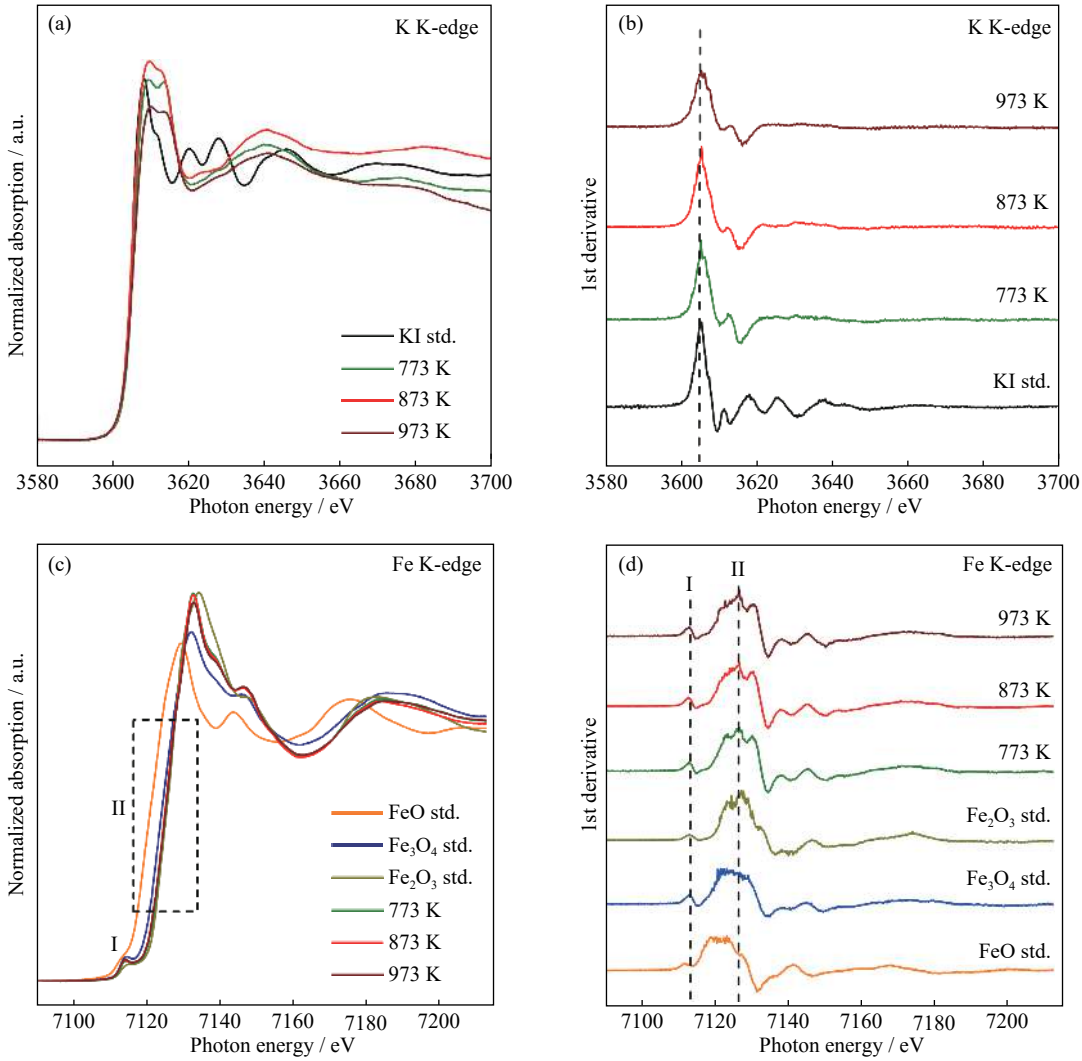

Fig. 5. Normalized XANES spectra at K K-edge (a) and Fe K-edge (c), including their 1st derivative plots at K K-edge (b) and Fe K-edge (d) of $KFeO_2$ samples calcined at 773, 873, and 973 K for 2 h.

of the high atomic concentration of C and low atomic concentration of Fe on the sample surface. Furthermore, the inset of Fig. 6(a) presents the hysteresis loops, suggesting weak ferromagnetism in all the calcined $KFeO_2$ samples. The data obtained from the hysteresis loops including coercivity (H_C), remanent magnetization (M_R), and squareness ratio (M_R/M_S) are summarized in Table 2. As presented in Table 2, the coercivity increases from 3.51 to 16.89 kA·m^{-1} with increasing calcination temperature from 773 to 973 K. In magnetic recording media application, a high H_C range of 47–95 kA·m^{-1} is required to keep the recording information for a long time [45]. Therefore, the synthesis of $KFeO_2$ nanoparticles is not suitable for application in recording media. For the squareness ratio, the value is between 0.06 and 0.11. Hence, the present investigation suggests a multi-domain structure in the materials because the value was below 0.5 [43].

Fig. 6(b)–(d) show the magnetization (M) measured as a function of temperature (T) between 50 and 350 K with an external magnetic field of 80 kA·m^{-1}. For the zero-field cooled (ZFC) measurement, the sample was first cooled to 50 K in the absence of the magnetic field. A field of 80 kA·m^{-1} was then applied, and the magnetization was measured as the sample was heated from 50 to 350 K. In contrast to the field cooled (FC) measurement, the sample was cooled to 50 K in the presence of the magnetic field of 80 kA·m^{-1}. Magnetization was then measured as the sample was cooled down. As shown in Fig. 6(b)–(c), the ZFC magnetization (M_{ZFC}) of the samples calcined at 773 and 873 K increases with increasing temperature from 50 K and then decreases after reaching the maximum value at the blocking temperature (T_B). The T_B values are estimated to be 125 and 85 K in the sample calcined at 773 and 873 K, respectively, whereas T_B could not observe in the sample calcined at 973 K as seen in Fig. 6(d). Moreover, T_B tends to decrease with increasing calcination temperature. The decrease in M_{ZFC} with the increase of the temperature after reaching the maximum T_B may be explained as that the thermal energy became large enough to cause the magnetic moments to flip randomly, resulting in a suppression of the magnetization of the particles [44]. For the FC magnetization (M_{FC}), the magnetization steadily decreases as temperature increases from 50 to 350 K. The overlap between M_{ZFC} and M_{FC} is observed at the temperature over the corresponding T_B and no overlapping is obviously observed in the sample calcined at 973 K. The existence of energy

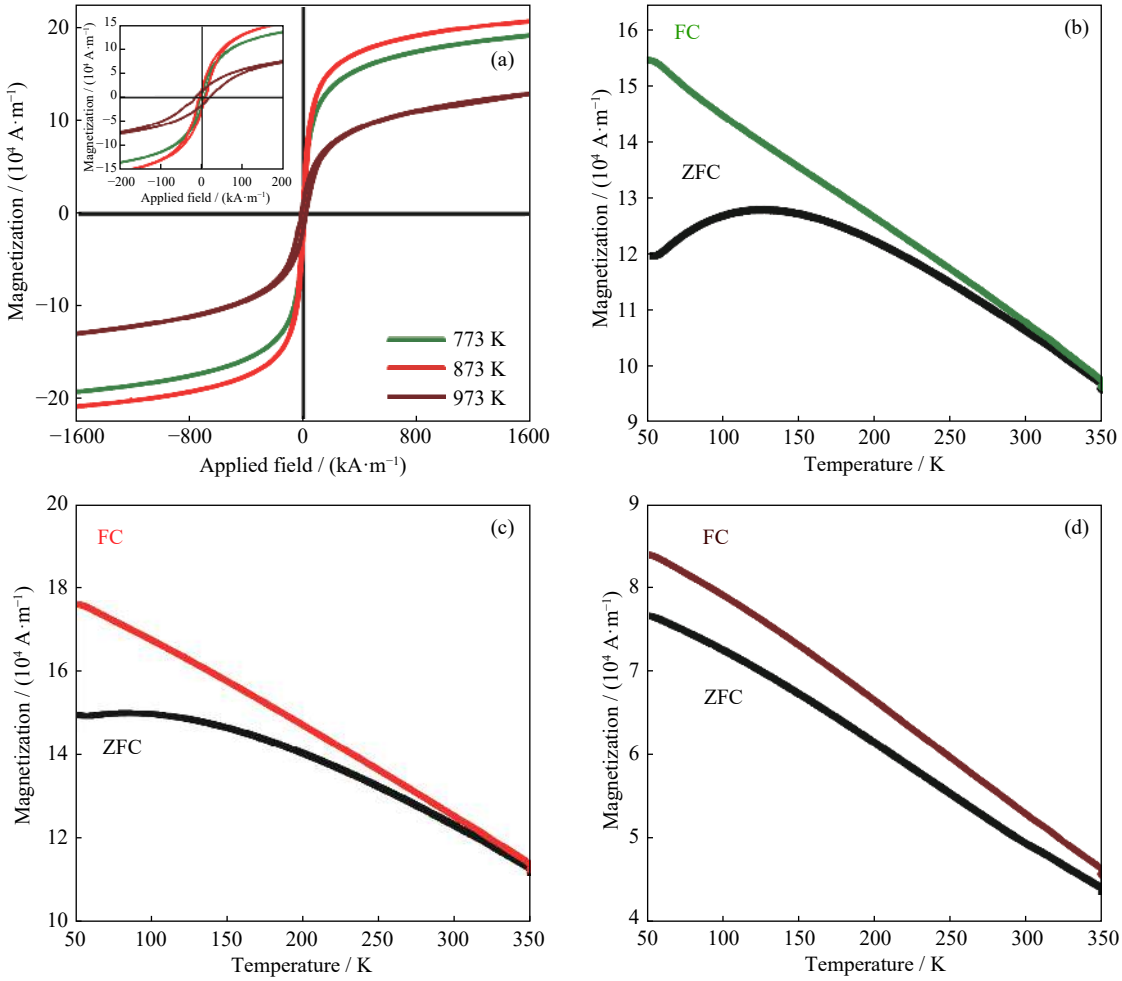

Fig. 6. (a) Magnetization as a function of applied magnetic field measured at room temperature (inset presents the hysteresis loops) and zero-field cooled (ZFC) and field cooled (FC) magnetization measured as a function of temperature (K) at an external field of 80 kA·m^{-1} of the $KFeO_2$ samples calcined at (b) 773 K, (c) 873 K, and (d) 973 K, respectively.

Table 2. Hysteresis loops obtained from VSM measurement of the synthesized $KFeO_2$ samples calcined at different temperatures

Calcined temperature / K	M_S at ±1600 kA·m^{-1} / (A·m^{-1})	H_C / (kA·m^{-1})	M_R / (A·m^{-1})	M_R/M_S
773	1.93×10^4	3.51	1.15×10^3	0.06
873	2.07×10^4	6.89	2.13×10^3	0.10
973	1.30×10^4	16.89	1.42×10^3	0.11

barriers of magnetic anisotropy results in the difference between M_{ZFC} and M_{FC} to fall below T_B [46]. On the basis of the above results, there are two possible reasons that explain the reduction of M_S: (i) the existence of the non-magnetic surface due to a high atomic concentration of carbon at the particle surface [47]; (ii) the high surface-to-volume ratio in the small particles caused spin canting at the surface [48].

4. Conclusion

In this research, we successfully synthesized $KFeO_2$ nanoparticles by using a simple, cost effective, and eco-friendly egg white solution method. The use of egg white proteins in gel form serves as capping agent for the synthesis of $KFeO_2$ nanoparticles upon calcination at 773, 873, and 973 K. XRD results confirmed the phase formation of $KFeO_2$ at different calcination temperatures. TEM revealed that the particle size of the synthesized $KFeO_2$ strongly depends on the calcination temperature. XPS results confirmed the chemical compositions on the $KFeO_2$ sample surface, and the calculated atomic concentrations correlated well with their magnetic properties. At room temperature, all of the synthesized $KFeO_2$ samples were ferromagnetic, with the highest M_S of 2.07×10^4 A·m^{-1}. Therefore, the synthesized $KFeO_2$ nanoparticles may be considered as a potential material for biomedical applications due to their high saturation magnetization and weak ferromagnetic behavior at room temperature.

Acknowledgements

The authors gratefully acknowledge the contributions to this work: Khon Kaen University and the Synchrotron Light Research Institute (BL 5.2 and BL 5.3), Thongsuk Sichumsaeng would like to thank the Science Achievement Scholar-

ship of Thailand (SAST) for the support of her PhD study. This work was supported by Suranaree University of Technology (SUT) and was financially supported by the Office of the Higher Education Commission under NRU Project of Thailand and the Research Network NANOTEC (RNN) program of the National Nanotechnology Center (NANOTEC), NSTDA, Ministry of Higher Education, Science, Research and Innovation (MHESI), Thailand.

Conflict of Interest

The authors declare no potential conflict of interest.

References

[1] H. Shokrollahi, A review of the magnetic properties, synthesis methods and applications of maghemite, *J. Magn. Magn. Mater.*, 426(2017), p. 74.

[2] S. Bharadwaj, A. Tirupathi, N. Pavan Kumar, S. Pola, and Y. Kalyana Lakshmi, Study of magnetic and magnetoresistance behaviour of $La_{0.67}Sr_{0.33}MnO_3$–$CoFe_2O_4$ composites, *J. Magn. Magn. Mater.*, 513(2020), art. No. 167058.

[3] S. Munjal, N. Khare, B. Sivakumar, and D. Nair Sakthikumar, Citric acid coated $CoFe_2O_4$ nanoparticles transformed through rapid mechanochemical ligand exchange for efficient magnetic hyperthermia applications, *J. Magn. Magn. Mater.*, 477(2019), p. 388.

[4] S. Talukdar, P. Saha, I. Chakraborty, and K. Mandal, Surface functionalized $CoFe_2O_4$ nano-hollowspheres: Novel properties, *J. Magn. Magn. Mater.*, 513(2020), art. No. 167079.

[5] P. Abasian, M. Radmansouri, M. Habibi Jouybari, M.V. Ghasemi, A. Mohammadi, M. Irani, and F.S. Jazi, Incorporation of magnetic NaX zeolite/DOX into the PLA/chitosan nanofibers for sustained release of doxorubicin against carcinoma cells death *in vitro*, *Int. J. Biol. Macromol.*, 121(2019), p. 398.

[6] F. Sharifianjazi, M. Moradi, N. Parvin, A. Nemati, A. Jafari Rad, N. Sheysi, A. Abouchenari, A. Mohammadi, S. Karbasi, Z. Ahmadi, A. Esmaeilkhanian, M. Irani, A. Pakseresht, S. Sahmani, and M. Shahedi Asl, Magnetic $CoFe_2O_4$ nanoparticles doped with metal ions: A review, *Ceram. Int.*, 46(2020), No. 11, p. 18391.

[7] A. Abuchenari and M. Moradi, Effect of Cu-substitution on the microstructure and magnetic properties of Fe–15%Ni alloy prepared by mechanical alloying, *J. Compos. Compd.*, 1(2019), No. 1, p. 13.

[8] A.R. Rouhani, A.H. Esmaeil-Khanian, F. Davar, and S. Hasani, The effect of agarose content on the morphology, phase evolution, and magnetic properties of $CoFe_2O_4$ nanoparticles prepared by sol–gel autocombustion method, *Int. J. Appl. Ceram. Technol.*, 15(2018), No. 3, p. 758.

[9] M. Kim, B.H. Kim, H.C. Choi, and B.I. Min, Origin of high Néel temperature in the low coordination number system AFeO$_2$(A=K and Rb), *Phys. Rev. B*, 81(2010), No. 21, art. No. 212405.

[10] K. Edström, S. Ito, and R.G. Delaplane, The crystal and magnetic structure of nonstoichiometric K^+ β-ferrite, *J. Magn. Magn. Mater.*, 212(2000), No. 3, p. 347.

[11] M. Tabuchi, Preparation of AFeO$_2$ (A = Li, Na) by hydrothermal method, *Solid State Ionics*, 79(1995), p. 220.

[12] A. Kotarba, A. Barański, S. Hodorowicz, J. Sokołowski, A. Szytuła, and L. Holmlid, Stability and excitation of potassium promoter in iron catalysts – The role of $KFeO_2$ and $KAlO_2$ phases, *Catal. Lett.*, 67(2000), No. 2-4, p. 129.

[13] S.C. Han, W.B. Park, K.S. Sohn, and M. Pyo, $KFeO_2$ with corner-shared FeO_4 frameworks as a new type of cathode material in potassium-ion batteries, *J. Solid State Electrochem.*, 23(2019), No. 11, p. 3135.

[14] A.K. Tangra, S. Singh, N.X. Sun, and G.S. Lotey, Investigation of structural, Raman and photoluminescence properties of novel material: $KFeO_2$ nanoparticles, *J. Alloys Compd.*, 778(2019), p. 47.

[15] L. Khanna and N.K. Verma, Synthesis, characterization and biocompatibility of potassium ferrite nanoparticles, *J. Mater. Sci. Technol.*, 30(2014), No. 1, p. 30.

[16] V.K. Garg, V.K. Sharma, and E. Kuzmann, Purification of water by ferrites - Mini review, [in] V.K. Sharma, R.A. Doong, H. Kim, R.S. Varma, and D.D. Dionysiou eds., *Ferrites and Ferrates: Chemistry and Applications in Sustainable Energy and Environmental Remediation*, American Chemical Society, Washington, DC, 2016, p. 137.

[17] L. Khanna and N. Kumar Verma, Study on novel, superparamagnetic and biocompatible PEG/$KFeO_2$ nanocomposite, *J. Appl. Biomed.*, 13(2015), No. 1, p. 23.

[18] L. Khanna and N.K. Verma, Silica/potassium ferrite nanocomposite: Structural, morphological, magnetic, thermal and *in vitro* cytotoxicity analysis, *Mater. Sci. Eng. B*, 178(2013), No. 18, p. 1230.

[19] B.S. Randhawa, H.S. Dosanjh, and N. Kumar, Synthesis of potassium ferrite by precursor and combustion methods, *J. Therm. Anal. Calorim.*, 95(2009), No. 1, p. 75.

[20] A. Kotarba, W. Bieniasz, P. Kuśtrowski, K. Stadnicka, and Z. Sojka, Composite ferrite catalyst for ethylbenzene dehydrogenation: Enhancement of potassium stability and catalytic performance by phase selective doping, *Appl. Catal. A*, 407(2011), No. 1-2, p. 100.

[21] S.J. Moon, I.B. Shim, and C.S. Kim, Crystallographic and magnetic properties of $KFeO_2$, *IEEE Trans. Magn.*, 42(2006), No. 10, p. 2879.

[22] C. Masingboon, S. Maensiri, T. Yamwong, P.L. Anderson, and S. Seraphin, Nanocrystalline $CaCu_3Ti_4O_{12}$ powders prepared by egg white solution route: Synthesis, characterization and its giant dielectric properties, *Appl. Phys. A*, 91(2008), No. 1, p. 87.

[23] B.L. Cushing, V.L. Kolesnichenko, and C.J. O'Connor, Recent advances in the liquid-phase syntheses of inorganic nanoparticles, *Chem. Rev.*, 104(2004), No. 9, p. 3893.

[24] S. Bagheri, K. Shameli, and S.B. Abd Hamid, Synthesis and characterization of anatase titanium dioxide nanoparticles using egg white solution via sol–gel method, *J. Chem.*, 2013(2013), art. No. 848205.

[25] M.A. Lambrecht, L.J. Deleu, I. Rombouts, and J.A. Delcour, Heat-induced network formation between proteins of different sources in model systems, wheat-based noodles and pound cakes, *Food Hydrocolloids*, 79(2018), p. 352.

[26] I. van der Plancken, A. van Loey, and M.E.G. Hendrickx, Changes in sulfhydryl content of egg white proteins due to heat and pressure treatment, *J. Agric. Food Chem.*, 53(2005), No. 14, p. 5726.

[27] S. Renzetti, I.A.F. van den Hoek, and R.G.M. van der Sman, Amino acids, polyols and soluble fibres as sugar replacers in bakery applications: Egg white proteins denaturation controlled by hydrogen bond density of solutions, *Food Hydrocolloids*, 108(2020), art. No. 106034.

[28] N. Hagolle, P. Relkin, Y. Popineau, and D. Bertrand, Study of the stability of egg white protein-based foams: Effect of heating protein solution, *J. Sci. Food Agric.*, 80(2000), No. 8, p. 1245.

[29] S. Dhara, Synthesis of nanocrystalline alumina using egg white, *J. Am. Ceram. Soc.*, 88(2005), No. 7, p. 2003.

[30] K. Thiyagarajan, V.K. Bharti, S. Tyagi, P.K. Tyagi, A. Ahuja, K. Kumar, T. Raj, and B. Kumar, Synthesis of non-toxic, biocompatible, and colloidal stable silver nanoparticle using

egg-white protein as capping and reducing agents for sustainable antibacterial application, *RSC Adv.*, 8(2018), No. 41, p. 23213.

[31] V. Petříček, M. Dušek, and L. Palatinus, Crystallographic computing system JANA2006: General features, *Z. Kristallogr. - Cryst. Mater.*, 229(2014), No. 5, p. 345.

[32] N.V. Proskurnina, V.I. Voronin, G.S. Shekhtman, L.N. Maskaeva, N.A. Kabanova, A.A. Kabanov, and V.A. Blatov, Ionic conductivity in Ti-doped $KFeO_2$: Experiment and mathematical modeling, *J. Phys. Chem. C*, 121(2017), No. 39, p. 21128.

[33] P. Muhammed Shafi and A. Chandra Bose, Impact of crystalline defects and size on X-ray line broadening: A phenomenological approach for tetragonal SnO_2 nanocrystals, *AIP Adv.*, 5(2015), No. 5, art. No. 057137.

[34] E.S. Freeman, The kinetics of the thermal decomposition of potassium nitrate and of the reaction between potassium nitrite and Oxygen, *J. Am. Chem. Soc.*, 79(1957), No. 4, p. 838.

[35] B.H. Toby, R factors in Rietveld analysis: How good is good enough?, *Powder Diffr.*, 21(2006), No. 1, p. 67.

[36] X.Y. Li, C.F. Liu, C.K. Zhang, H.Y. Fu, X.H. Nan, W.D. Ma, Z.Y. Li, K. Wang, H.B. Wu, and G.Z. Cao, Effects of preinserted Na ions on Li-ion electrochemical intercalation properties of V_2O_5, *ACS Appl. Mater. Interfaces*, 8(2016), No. 37, p. 24629.

[37] Z.J. Huang, Z.X. Wang, X.B. Zheng, H.J. Guo, X.H. Li, Q. Jing, and Z.H. Yang, Structural and electrochemical properties of Mg-doped nickel based cathode materials $LiNi_{0.6}Co_{0.2}Mn_{0.2-x}Mg_xO_2$ for lithium ion batteries, *RSC Adv.*, 5(2015), No. 108, p. 88773.

[38] M.H. Pham, C.T. Dinh, G.T. Vuong, N.D. Ta, and T.O. Do, Visible light induced hydrogen generation using a hollow photocatalyst with two cocatalysts separated on two surface sides, *Phys. Chem. Chem. Phys.*, 16(2014), No. 13, p. 5937.

[39] T. Gholam, L.R. Zheng, J.O. Wang, H.J. Qian, R. Wu, and H.Q. Wang, Synchrotron X-ray absorption spectroscopy study of local structure in Al-doped $BiFeO_3$ powders, *Nanoscale Res. Lett.*, 14(2019), No. 1, art. No. 137.

[40] G. Kataby, Y. Koltypin, J. Rothe, J. Hormes, I. Felner, X. Cao, and A. Gedanken, The adsorption of monolayer coatings on iron nanoparticles: Mössbauer spectroscopy and XANES results, *Thin Solid Films*, 333(1998), No. 1-2, p. 41.

[41] T.E. Westre, P. Kennepohl, J.G. DeWitt, B. Hedman, K.O. Hodgson, and E.I. Solomon, A multiplet analysis of Fe K-edge 1s → 3d pre-edge features of iron complexes, *J. Am. Chem. Soc.*, 119(1997), No. 27, p. 6297.

[42] P.A. Bingham, O.M. Hannant, N. Reeves-Mclaren, M.C. Stennett, and R.J. Hand, Selective behaviour of dilute Fe^{3+} ions in silicate glasses: An Fe K-edge EXAFS and XANES study, *J. Non Cryst. Solids*, 387(2014), p. 47.

[43] G. Mustafa, M.U. Islam, W.L. Zhang, Y. Jamil, M. Asif Iqbal, M. Hussain, and M. Ahmad, Temperature dependent structural and magnetic properties of Cerium substituted Co–Cr ferrite prepared by auto-combustion method, *J. Magn. Magn. Mater.*, 378(2015), p. 409.

[44] B. Issa, I.M. Obaidat, B.A. Albiss, and Y. Haik, Magnetic nanoparticles: Surface effects and properties related to biomedicine applications, *Int. J. Mol. Sci.*, 14(2013), No. 11, p. 21266.

[45] Y.D. Li, R.M. Liu, Z.D. Zhang, and C.S. Xiong, Synthesis and characterization of nanocrystalline $BaFe_{9.6}Co_{0.8}Ti_{0.8}M_{0.8}O_{19}$ particles, *Mater. Chem. Phys.*, 64(2000), No. 3, p. 256.

[46] T. Hyeon, Y. Chung, J. Park, S.S. Lee, Y.W. Kim, and B.H. Park, Synthesis of highly crystalline and monodisperse cobalt ferrite nanocrystals, *J. Phys. Chem. B*, 106(2002), No. 27, p. 6831.

[47] R.D. Sánchez, J. Rivas, P. Vaqueiro, M.A. López-Quintela, and D. Caeiro, Particle size effects on magnetic properties of yttrium iron garnets prepared by a sol–gel method, *J. Magn. Magn. Mater.*, 247(2002), No. 1, p. 92.

[48] J.S. Lee, J.M. Cha, H.Y. Yoon, J.K. Lee, and Y.K. Kim, Magnetic multi-granule nanoclusters: A model system that exhibits universal size effect of magnetic coercivity, *Sci. Rep.*, 5(2015), art. No. 12135.